Structural investigation and site selective emission on Eu^{3+} activated CaF_2 and SrF_2 nanoparticles: effect of the particle size and co-doping with alkaline ions

Paolo Cortelletti[a], Marco Pedroni[a], Federico Boschi[b], Sonia Pin[c], Paolo Ghigna[c], Patrizia Canton[d], Fiorenzo Vetrone[e,f], Adolfo Speghini[a]*

[a] Nanomaterials Research Group, Dipartimento di Biotecnologie, Università di Verona and INSTM, UdR Verona, Strada Le Grazie 15, I-37134 Verona, Italy

[b] Dipartimento di Informatica, Università di Verona, Strada Le Grazie 15, I-37134 Verona, Italy

[c] Dipartimento di Chimica, Università di Pavia and INSTM, UdR Pavia, V.le Taramelli 16, I-27100, Pavia, Italy

[d] Centro di Microscopia Elettronica "Giovanno Stevanato", Department of Molecular Sciences and Nanosystems, Ca' Foscari University of Venice, Via Torino 155/B, Venezia-Mestre, Italy

[e] Institut National de la Recherche Scientifique, Centre Énergie, Matériaux et Télécommunications (INRS - EMT), Université du Québec, 1650 Boul. Lionel-Boulet, Varennes, QC, J3X 1S2 (Canada)

[f] Centre for Self-Assembled Chemical Structures (CSACS), McGill University, Montréal, H3A 2K6, Québec, Canada

[†] Corresponding Author: adolfo.speghini@univr.it

ABSTRACT

Eu^{3+} doped CaF_2 and SrF_2 nanoparticles were synthesized through a facile hydrothermal technique, using citrate ions as capping agents and Na^+ or K^+ as charge compensator ions. Tuning of the reaction time modulates the NP size, from few to several tens of nanometers. EXAFS spectra indicate that the Eu^{3+} ions enter the fluorite CaF_2 and SrF_2 structure as substitutional defects on the metal site, as confirmed by emission properties. Laser site selective spectroscopy demonstrated that the Eu^{3+} ions are mainly accommodated in two sites of different symmetry. The ion distribution in the particle depends on the NP size, as Eu^{3+} high symmetry sites are prevalent for bigger nanoparticles. Eu^{3+} ions in high symmetry sites show $^5D_0$ level lifetimes longer than 20 ms, amongst the longest lifetimes found in the literature for Eu^{3+} activated materials. As a proof of concept of possible use of the nanoparticles in nanomedicine, the red luminescence generated by two-photon absorption has been detected using pulsed laser excitation at 790 nm in the first biological window. The very long lifetimes indicate that the nanoparticles are interesting candidates for time resolved fluorescence techniques in biomedical imaging, as FLIM, for which fast autofluorescence is a drawback to avoid.

1. INTRODUCTION

The importance of lanthanide doped luminescent inorganic nanoparticles (NPs) has continuously grown in the past few years as their optical and paramagnetic features allow for many potential technological applications in several fields. In nanosized form, they have been found to be useful as optical labels and probes for biomedical applications as well as in photovoltaic devices.[1-6] Upconverting NPs, presenting emissions at higher energies with respect to the excitation radiation, have been widely investigated for their possible use in many modern technological applications, in particular where near-infrared excitation light is required[7, 8]. In particular, fluorides are excellent hosts for doping with luminescent ions, as they have low phonon energies and therefore low non-radiative relaxation processes. Among fluoride hosts, trivalent lanthanide (Ln^{3+}) doped alkaline-earth fluorides with the fluorite structure, such as CaF_2 and SrF_2, show interesting upconversion emission, and can be prepared by facile and environmental friendly methods as well.[9-12] The local environments of Ln^{3+} ions as dopants in single crystal alkaline-earth fluorides have been previously investigated [13-15]. However, a detailed study of the local environment for Ln^{3+} ions in nanoscale systems to understand their luminescence properties is lacking. For this purpose, the Eu^{3+} ion is an excellent luminescent probe to investigate the site symmetry in which the lanthanide ions are accommodated[16-18]. Although some reports have appeared in the literature on the spectroscopic properties of Eu^{3+} doped CaF_2 and SrF_2 nanoparticles[11, 19], a detailed investigation of the sites occupied by the Ln^{3+} ions in the crystal structure for nanocrystalline hosts deserves to be investigated since it can lead to better insight into the tuning of the luminescence properties. Moreover, understanding the effect of co-doping of these Ln^{3+} doped nanoparticles with alkali metal ions as charge compensators[20] is essential as it can lead to further modulation of their light emission properties. Some charge compensating mechanisms have been proposed in CaF_2 and SrF_2

single crystals, and lead to the formation of Ln^{3+} sites with C_{3v} or C_{4v} symmetry in the case of local charge compensation, and to sites with O_h symmetry in the case of non-local charge compensation. The presence of interstitial F^- ions also induces a distortion in the lattice structure due to the repulsion between the F^- ions.[20-23]

The nanocrystalline samples under investigation were prepared with a facile method involving the use of citrate groups as hydrophilic capping agents, to ensure excellent dispersion in water. Moreover, Na^+ or K^+ ions were chosen as counter ions of the citrate group to provide charge compensation[24-26]. The local chemical environment of Eu^{3+} was investigated by optical as well Extended X-ray Absorption Fine Structure (EXAFS) spectroscopies. The excited state dynamics for the Eu^{3+} ions were also investigated, by monitoring the emission decay of the luminescence. It is also worth mentioning that the Eu^{3+} ion is not only an excellent ion to investigate the site symmetry from a fundamental point of view but its red emission is also very useful for imaging purposes. We have also investigated the possible use of the present colloidal NPs using two-photon emission spectroscopy in the first biological window.

2. EXPERIMENTAL SECTION

2.1 Synthesis

Eu^{3+} ions doped MF_2 ($M=Ca^{2+}$, Sr^{2+}) NPs were prepared using a hydrothermal synthesis using a nominal $M:Eu^{3+}$ molar ratio of 0.99:0.01. Stoichiometric quantities of $CaCl_2 \cdot 2H_2O$ (Baker, >99%) or $SrCl_2 \cdot 6H_2O$ (Carlo Erba, >99%), $EuCl_3 \cdot 6H_2O$ (Aldrich, 99.99%), (total metal amount of $3.5 \cdot 10^{-3}$ mol), were dissolved in 5.0 ml of deionized water in a Teflon vessel. 20.0 ml of a 1.00 M sodium citrate (Na-cit) or potassium citrate (K-cit) (Fluka, ≥ 99%) solution was added under vigorous

stirring for 5 minutes. A 3.5 M aqueous solution of NH_4F (Baker, 99%) was added to the previous suspension, in order to have an excess of fluoride ions with respect to the stoichiometric amounts, (M+Eu):F=1:2.5. The obtained clear solution was transferred to a Teflon lined autoclave (DAB-2, Berghof) and heat treated at 190 °C under autogenous pressure. Several reaction times (10, 35, 360 and 480 minutes) were used in order to prepare samples with different particle sizes. The autoclave was then cooled to room temperature and after centrifugation (at 7000 rpm, for 10 min), the doped CaF_2 or SrF_2 NPs were collected and stored under acetone. The NPs can be easily dispersed in water as well as in saline solution to form transparent colloids. To obtain the NPs in powder form, the gel pellets were dried at room temperature for 24 h. For the sake of simplicity, the samples will be hereafter denoted as CN[reaction time, min] for CaF_2 NPs or SN[reaction time, min] for SrF_2 NPs prepared with sodium citrate as starting reagent. Moreover, CK[reaction time, min] is defined for SrF_2 NPs prepared with potassium citrate as starting reagent.

2.2 X-Ray powder diffraction measurements

X-Ray powder diffraction (XRPD) patterns were recorded with a Thermo ARL X´TRA powder diffractometer in Bragg-Brentano geometry, equipped with a Cu-anode X-ray source (K_α, λ=1.5418 Å) and a Si(Li) solid state detector. The patterns were collected with a scan rate of 2.5°/s and 2θ range of 20°-90°. The phase identification was performed with PDF-4+ 2009 database provided by the International Centre for Diffraction Data (ICDD). The instrumental X-Ray peak broadening was determined using LaB_6 standard reference material (SRM 660a) provided by NIST and the cell parameters were determined using an α-SiO_2 as an internal standard. The samples were carefully homogenized in a mortar, and deposited in a low-background sample stage. XRPD patterns are shown in the Supporting Information section.

2.3 Transmission Electron Microscopy

Transmission Electron Microscopy (TEM) and high resolution TEM (HRTEM) images were measured using a JEOL 3010 high resolution electron microscope (0.17 nm point-to-point resolution at Scherzer defocus), operating at 300 KV, equipped with a Gatan slow-scan CCD camera (model 794) and an Oxford Instrument EDS microanalysis detector (Model 6636). The powders were dispersed in water in order to be deposited on Holey-Carbon Copper grids.

2.4 Spectroscopy measurements

Luminescence spectra were measured with a Nd:YAG pumped tunable dye laser. The emission signal was analyzed by a half-meter monochromator (HR460, Jobin Yvon) equipped with a 1200 g/mm grating and detected with a CCD detector (Spectrum One, Jobin Yvon) with a spectral resolution of 0.15 nm. Emission decays were measured using a GaAs photomultiplier and a 500 MHz digital oscilloscope. 77 K emission spectra were acquired with an in house built L-N_2 immersion cold finger cryostat. Excitation spectra were acquired using a Fluorolog-3 (Horiba-Jobin Yvon), spectrophotometer, with a spectral resolution of 0.2 nm.

2.5 ICP-MS

ICP-MS analysis was carried out with a Thermo Fisher Scientific model X Series II equipped with a technology collision/reaction cell (CCT). The citrate groups and alkaline ions were completely removed from the NPs surface by washing the powder samples several times with a 0.5% HNO_3 solution. The obtained NPs were then dissolved in a 5% nitric acid solution.

2.6 EXAFS spectra

The EXAFS spectra at the Ln–K edges were measured as a function of the temperature in the range 300-20 K at the BM23 beamline of the European Synchrotron Radiation Facility (ESRF, Grenoble, Experiment CH-2330), in fluorescence mode, using a 13 element Ge detector for the fluorescence signal, and a double crystal Si(511) monochromator. For the measurements, a proper amount of sample (ca 0.3 g) intended to give the maximum contrast at the Ln-K edge was thoroughly mixed with cellulose in an agate mortar and then pressed to a pellet. For the EXAFS data analysis, at all the investigated edges, the EXAFS were extracted using the ATHENA code. The data analysis was performed using the EXCURVE program. Phases and amplitudes were calculated using the muffin-tin approximation, in the framework of the Hedin–Lundquist and Von Bart approximations for the exchange and ground state potentials, respectively: this includes the effects of inelastic losses due to the electron inelastic scattering (photoelectron mean free path). The fittings were done in the k space, using a k^2 weighting scheme, and full multiple scattering calculations within the cluster used in the fits (see below). The stability of the fits was verified by testing different weighting schemes and validating that the fitting parameters were recovered within the errors. The S_0^2 parameter, which provides a measure of events such as two-electron transitions (where the energy difference between the photon and the photoelectron is so large that they are not seen in the spectrum), was always found to be unity within the error: this was expected, as multi-channel events are included in the Hedin–Lundquist approximation. The accuracy of the phase shifts and amplitudes were tested by fitting the CeO_2 Ce–K edge EXAFS spectra, and recovering the crystallographic distances within 0.01 Å.

2.7 Two Photon Excitation

A two-photon microscope DM-6000 CS (Leica) was used to perform optical imaging of the NPs. The samples were excited by a Chameleon ULTRA II laser (Coherent) at 790 nm and visualized with a 20x objective (water immersed, numerical aperture of 1) in the range 570 – 650 nm. Acquisition and analysis of the images were done by using the LAS AF (Leica Application Suite Advance Fluorescence, Leica) software.

3. RESULTS AND DISCUSSION

3.1 Size and morphology

TEM measurements prove the growth of the NPs, as shown in Figure 1. The TEM micrographs show the monodisperse character of the NP size. From HREM images the crystallinity of the specimens is evident (as highlighted in Figure 1 by yellow circles), HREM of the single NPs shows the belonging to a Fm3m cubic structure. The effect of the different reaction times on the average size of the NPs is evident; in fact, there is a direct correlation between larger sizes and longer reaction times.

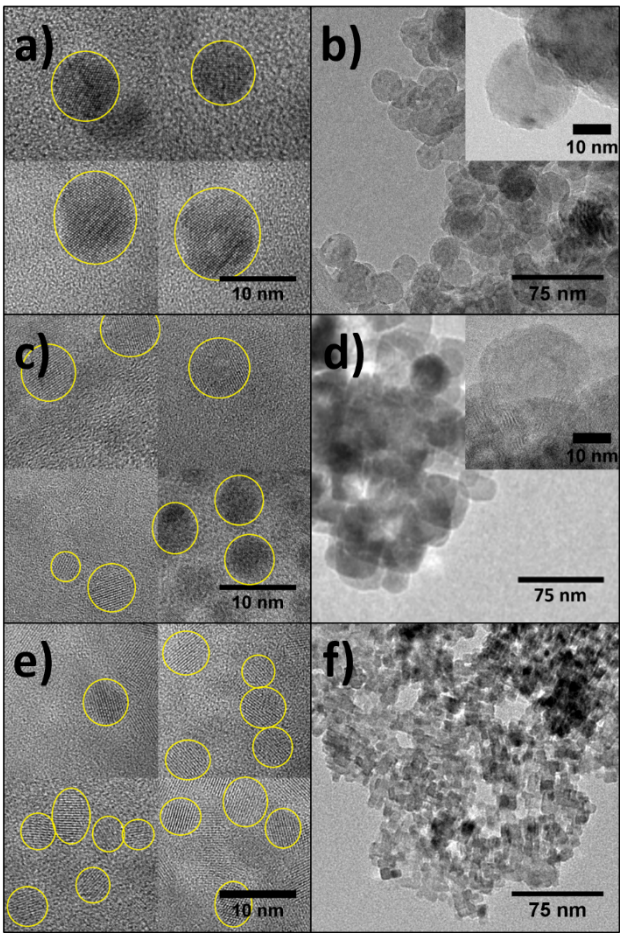

Figure 1. TEM images of a) CN10, b) CN480, c) CK10, d) CK480, e) SN10 and f) SN480 samples. To guide the eye, nanoparticles are delimited by yellow circles.

3.2 Structural details and EXAFS analysis

The elemental analysis and structural investigation are reported in the Supporting Information section. It was found that all the samples are single phase fluorite structure and that the size is clearly larger for NPs grown at longer reaction times, as also observed by TEM images shown in Figure 1. EXAFS spectra at the Eu-K edge at 20 K are shown in Figures 2 and 3, respectively, for the CN360 and SN360 samples. Visible EXAFS oscillations are present, above the noise level, up to k=14 $Å^{-1}$. Both spectra are better discussed by looking at the Fourier Transform (panel b). The

first peak (ca. 2.5 Å) is attributed to the 8 fluoride ions around the Ca, Sr site of the fluorite structure and the second peak, is attributed to Ca (Sr) atoms that are the next nearest neighbours. The spectra can then be fit using a fluorite structural model, in which the Nearest Neighbour (denoted as NN) shell is made up of 8 fluoride ions, and the Next Nearest Neighbour (denoted as NNN) shell is comprised of 12 Ca or Sr atoms.

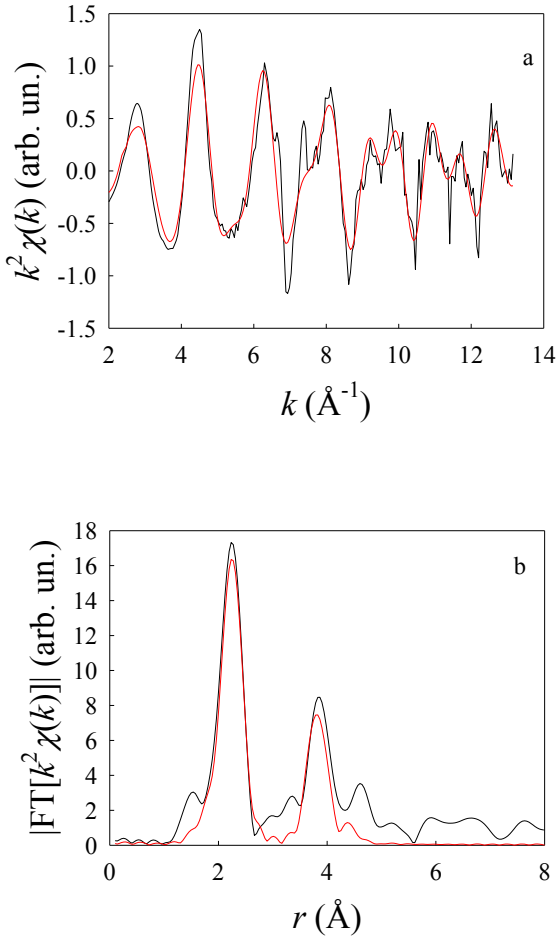

Figure 2. Eu-K edge spectrum of the CaF_2 doped sample at 20 K (a), and the corresponding Fourier transform. Black line: experimental; red line: fit according to the model described in text.

The results of the fit for the spectrum in Figure 3 are shown in Table 1. Concerning the Eu^{3+} doped CaF_2 sample, spectra have been measured as a function of temperature (T). The Eu-F and Eu-Ca distances are plotted as a function of T in Figure 4. It is clearly observed that Eu^{3+} doping induces a small structural disorder for what concerns both the NN (fluoride) shell and the NNN (calcium), the fitted distances being not dependent of T.

Table 1. EXAFS results for the spectrum in Fig. 3: ***n***: coordination number, ***r***: distance; σ^2: EXAFS Debye-Waller factor; r_0: crystallographic distance in SrF_2. *R*=11.6 %.

Shell	**Atom**	**n**	***r* (Å)**	**σ^2 (Å^2)**	**r_0 (Å)**
1	F	8	2.41(1)	$4(2)\times10^{-3}$	2.4738
2	Sr	12	4.12(1)	$3.3(7)\times10^{-3}$	4.0397

The Eu-F distance is slightly contracted compared to the Ca-F distance, as for the Eu^{3+} doped SrF_2 sample, in agreement with the ionic radii (1.07 Å for 8-fold coordinated Eu^{3+})[27]. In addition, the Eu-M distance is slightly increased both for the CaF_2 and for the SrF_2 samples. This can be related to the increased charge on Eu^{3+} compared to Ca^{2+} or Sr^{2+}. Finally, the trends of the EXAFS Debye-Waller (DW) factors as a function of T, are also shown in Figure 4. The upper panel shows the DW factor for the NN (fluoride), the lower panel for the next nearest neighbours (Ca). The continuous lines are fits using the Einstein model. A small amount of static disorder is found in both cases (5×10^{-4} and 1×10^{-3} Å^2, respectively). The Einstein temperatures are 433 K and 200 K, while the reduced masses agree quite well with those for the Eu-F and Eu-Ca couples.

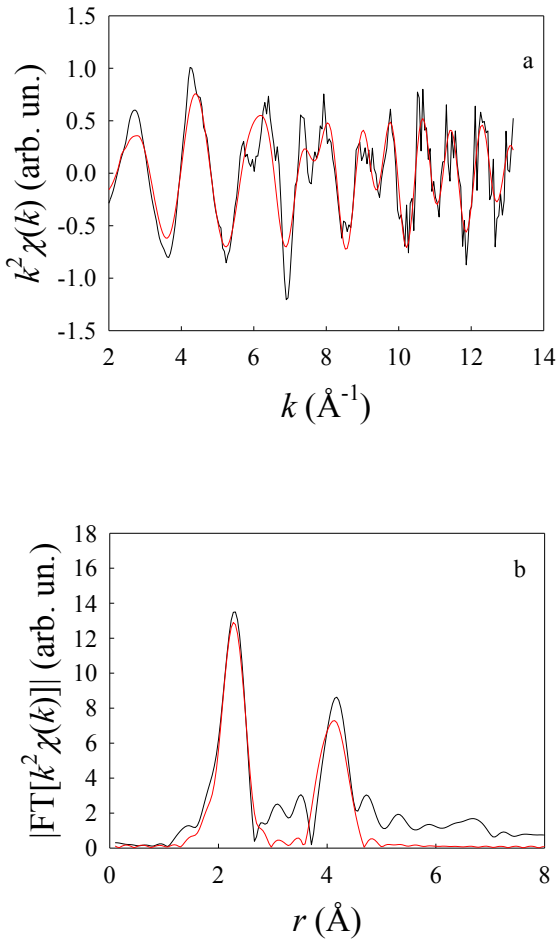

Figure 3. Eu-K edge spectrum of the SrF_2 doped sample at 20 K (a), and the corresponding Fourier transform. Black line: experimental; red line: fit according to the model described in text.

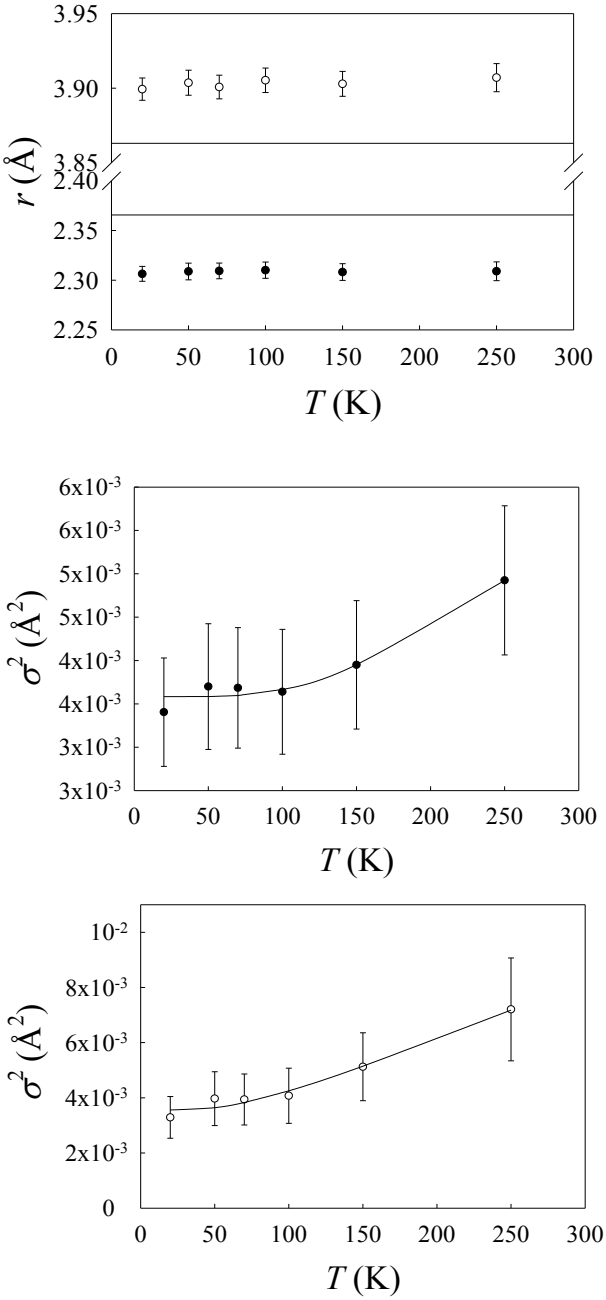

Figure 4. EXAFS fitting results for the Eu^{3+} doped CaF_2 sample as a function of T. Upper panel: distances; middle and lower panel: EXAFS Debye-Waller factors for the first and second shell, respectively. The horizontal lines in the upper panel correspond to the crystallographic distances in pure CaF_2. The continuous lines in the middle and lower panels are fits according to the Einstein model.

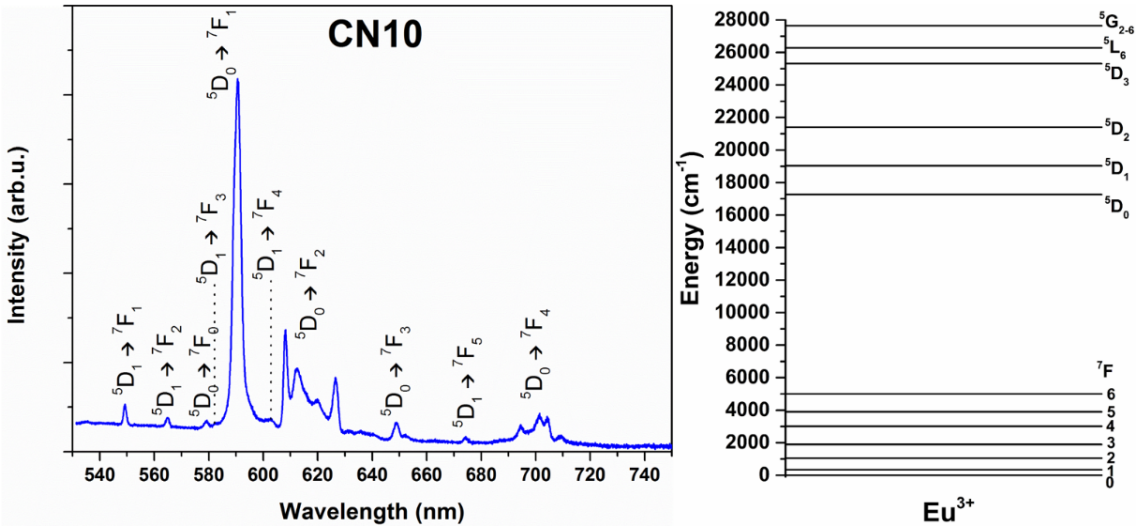

Figure 5. Emission spectrum of the CN10 sample upon 465 nm excitation (left) and corresponding energy level scheme for Eu^{3+} ions (right).

3.3 Spectroscopic investigation

3.3.1 Non-selective spectroscopy.

As demonstrated by the EXAFS results, the Eu^{3+} ions are substituting the Ca^{2+} or Sr^{2+} ions in the crystal structure and therefore a charge compensation mechanism is involved in the process[15, 23]. It was observed that the Na^+ and K^+ alkaline ions, present in the NPs preparation procedure, provided by sodium or potassium citrate reagents, can provide charge compensation[24, 28]. Due to this charge compensation, the Eu^{3+} ions can occupy sites with different symmetries and therefore, they are subjected to different crystal fields, that strongly influence their emission features. In fact, the Eu^{3+}emission is particularly dependent on the local symmetry[16, 23, 29], and this behaviour makes the Eu^{3+} ion an excellent structural probe. As an example, the emission spectrum of the CN10 sample upon 465 nm laser excitation is shown in Figure 5. The emission spectra for CK10 and SN10 samples are very similar to the CN10 one (see Figure S3, Supporting Information Section). As

shown in Figure 5, the emission spectrum presents the typical Eu^{3+} emission bands due to the $^5D_I \rightarrow {}^7F_J$ transitions. The strongest features are due to the $^5D_0 \rightarrow {}^7F_1$ and $^5D_0 \rightarrow {}^7F_2$ transitions, around 590 nm and 615 nm, respectively. The $^5D_0 \rightarrow {}^7F_1$ transition is a magnetic dipole transition and it is independent from the Eu^{3+} local environment, while the $^5D_0 \rightarrow {}^7F_2$ transition is an electric dipole (ED) transition, a so-called "*hypersensitive transition*" since its intensity strongly depends on the $U^{(2)}$ and $U^{(4)}$ reduced matrix elements. [29].

Room temperature excitation spectra have been measured considering emissions at 589 nm and 611 nm, corresponding to the $^5D_0 \rightarrow {}^7F_1$ and $^5D_0 \rightarrow {}^7F_2$ transitions, respectively, and they are shown in Figure 6. The excitation spectra show typical bands due to the Eu^{3+} ions, corresponding to transitions starting from the $^7F_0$ level to higher excited states. The strongest band centred at 395 nm is due to the $^7F_0 \rightarrow {}^5L_6$ transition. The excitation spectra for the two different emission wavelengths are different. For instance, the excitation band around 525 nm due to the $^7F_0 \rightarrow {}^5D_1$ transition appear to be stronger for the 589 nm emission than for the 611 nm one. Moreover, the excitation bands at the two different emission wavelengths due to the $^7F_0 \rightarrow {}^5D_2$ transition, which is an electric dipole hypersensitive transition[29], are different. The inset in Figure 6 clearly shows five Stark transitions, in the 455 to 475 range, in the case of the 589 nm emission, while for the excitation spectrum at 611 nm only one band located around 465 nm is observed. This behaviour is quite similar for CN10, CK10 and SN10 samples.

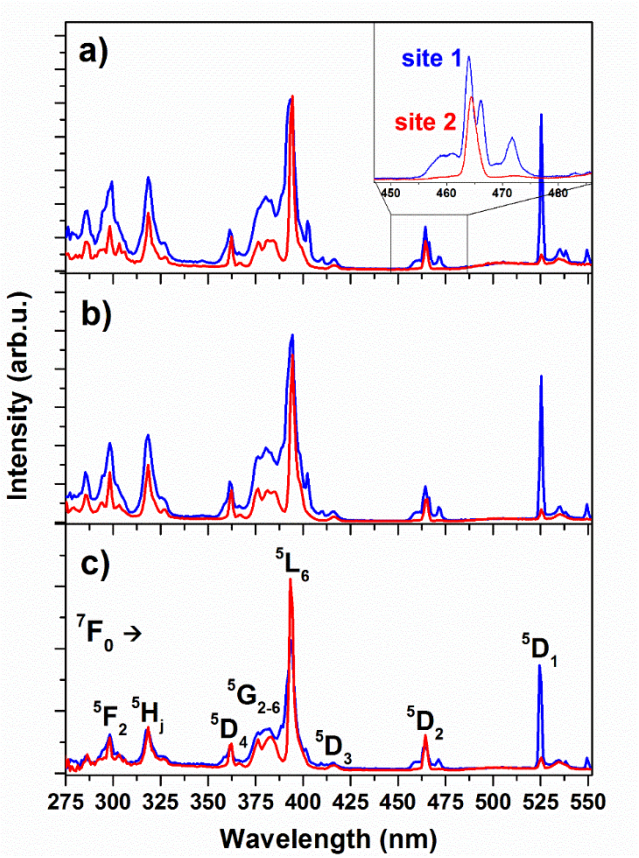

Figure 6. Room temperature excitation spectra for a) CN10, b) CK10, c) SN10 samples. Blue lines: 589 nm emission; red lines: 611 nm emission. Inset: $^7F_0 \rightarrow {}^5D_2$ transition for the CN10 sample. The spectra were acquired respecting the same experimental conditions, only the emission wavelength was changed.

These behaviours put into evidence the presence of at least two sites with different symmetry accommodating the Eu^{3+} ions, corresponding to different local crystal fields and generating different splitting of the $^5D_2$ Stark levels. The excitation site represented by the blue line in Figure 6 will be denoted hereafter as site 1, while the site represented by the red line will be denoted as site 2. Site 1 can be identified as the so-called P site indicated by Hamers et al.[15] for an Eu^{3+} doped

CaF_2 single crystal, since the two main Stark bands of its $^7F_0 \rightarrow {}^5D_2$ transition perfectly match the two excitation bands reported by Hamers et al. for this site at 464 nm and 466.5 nm. Hamers et al. also report on two excitation bands for the $^7F_0 \rightarrow {}^5D_1$ transition around 525.5 nm, separated by 0.2 nm. These bands are probably too close in energy to be separately observed with our instrumental setup. Moreover, site 2 can be identified with the so-called Q or R sites shown by Hamers consisting of Eu^{3+} dimers that present multiple Stark bands around 525.5 nm and 465 nm. The excitation bands for the $^7F_0 \rightarrow {}^5D_2$ and $^7F_0 \rightarrow {}^5D_1$ transitions, shown in Figure 6, cannot be assigned to a single Q or R site, most probably because the bands due to these sites are strongly overlapped, beyond the spectral resolution of our instrumental setup.

3.3.2 Site selective spectroscopy.

Considering the features observed in the excitation spectrum, we carried out site selection spectroscopy measurements using a tunable dye laser in the 455-475 nm range as the excitation source. The site selection spectroscopy emissions are shown in Figure 7. From the excitation spectrum (shown in Figure 6), it is observed that it is possible to select site 1 by exciting at 460 or 472 nm. On the other hand, site 2 can be partly selected, because its excitation band, peaked at 465 nm, partially overlaps the site 1 excitation band (see Figure 6). By tuning the laser energy at 461.0, the site 1 emission is collected and it shows a dominant $^5D_0 \rightarrow {}^7F_1$ band for all the samples under investigation (see Figure 7, blue lines), although features due to the other transitions are visible. On the other hand, after excitation at 464.5 nm, site 2 was mainly excited, and the intensity of the $^5D_0 \rightarrow {}^7F_2$ transition is comparable to the intensity of the $^5D_0 \rightarrow {}^7F_1$ transition, although contributions from both sites are present.

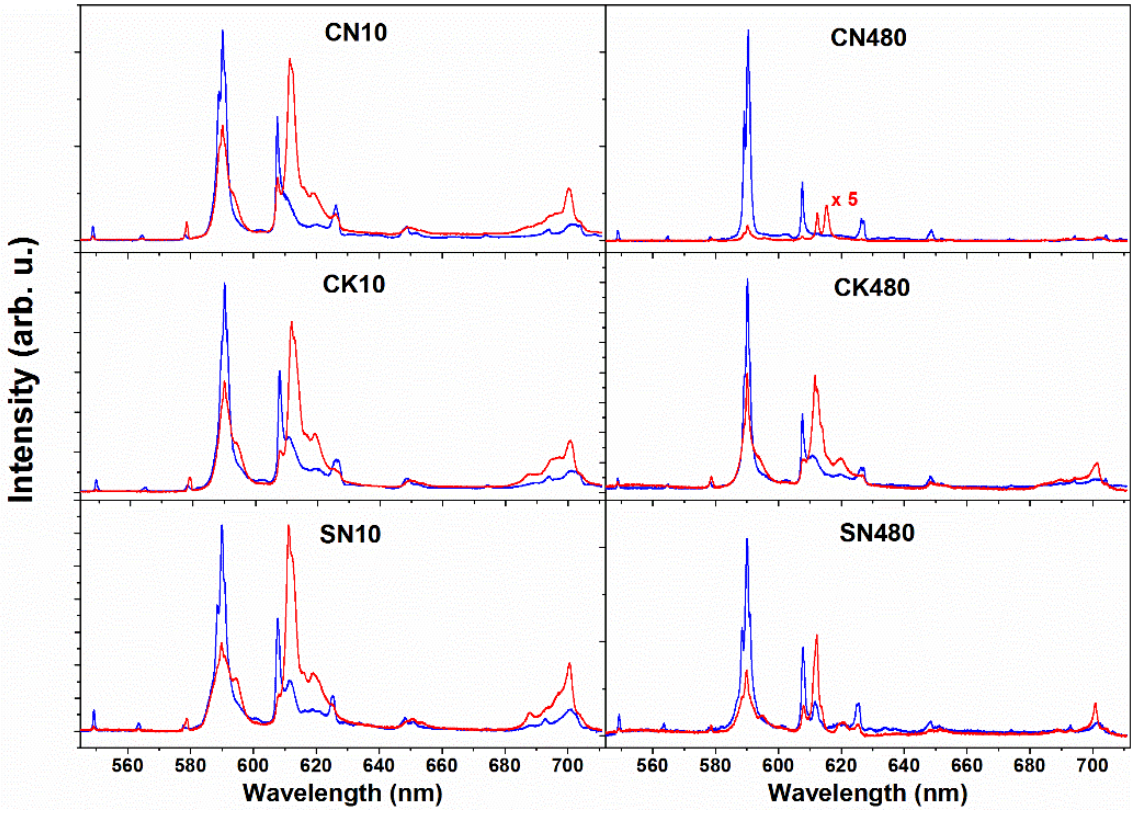

Figure 7. Site selection spectroscopy on the 10 min time reaction samples (left column) and 8 hour time reaction samples (right column). Blue spectra (λ_{exc} = 461.0 nm) are emissions from site 1 and red spectra (λ_{exc} = 464.5 nm) are emissions from site 2.

Site selective emissions for the other samples are shown in Figure S4 (Supporting Information Section). It is important to note that for site 1 emission, a contribution from site 2 is also present in all the emission spectra except for the CN480 sample, since the $^7F_0 \rightarrow {}^5D_2$ excitation band for site 2 shown in the inset in Figure 7 is extremely weak at 461.0 nm but not completely absent. Therefore, because of the laser power, site 2 can also be partially excited at 461.0 nm. The absence of site 2 contribution in the site selected emission of site 1 for the CN480 sample could be attributed to the fact that almost all Eu^{3+} ions are located in site 1 while only a few of them are located in site

2. This hypothesis is also supported by the extremely low site 2 emission with respect to site 1 emission for the CN480 sample.

From the observed emission spectra it is possible to make some inferences about the site symmetry surrounding the Eu^{3+} ions[13, 16, 29-31]. First, it can be noticed that for site 1 the $^5D_0 \rightarrow {}^7F_0$ transition is weak or almost absent, while for site 2 it is clearly observable around 580 nm. This transition is electric dipole forbidden, but thanks to the j-mixing effect[25] the emission is measurable. The presence of the $^5D_0 \rightarrow {}^7F_0$ band indicates that the possible site 2 local symmetries for the lanthanide ions are C_s, C_1, C_2, C_3, C_4, C_6, C_{2v}, C_{3v}, C_{4v}, and C_{6v}[16, 29]. Since the $^5D_0 \rightarrow {}^7F_0$ transition for site 1 is absent or very weak (probably because of contributions from site 2), it can be inferred that its symmetry is higher than for site 2.

Another clear feature of the emission spectra of all samples is that the relative intensity between the emission around 612 nm ($^5D_0 \rightarrow {}^7F_2$ transition) and 590 nm ($^5D_0 \rightarrow {}^7F_1$ transition) is different for excitation in the two different sites and it changes for samples prepared with increased reaction time. The ratio between the $^5D_0 \rightarrow {}^7F_2$ integrated intensity transition and the magnetic dipole $^5D_0 \rightarrow {}^7F_1$ one is called the asymmetry ratio, an indicator of the local Eu^{3+} symmetry [16, 29, 32], defined as

$$R = \frac{A_{612}}{A_{590}} \qquad (1)$$

where A_{612} is the integrated area of the 612 nm emission band and A_{590} is the integrated area of the 590 nm emission band. An increase of the asymmetry ratio points to a decrease of symmetry and vice-versa. The asymmetry ratio for site 1 was calculated for all the samples synthesized with different reaction times, and it is shown in Figure 8. Since site selection for site 2 was not possible because of the overlapping of its excitation spectra with the one of site 1, its asymmetry ratio was not calculated.

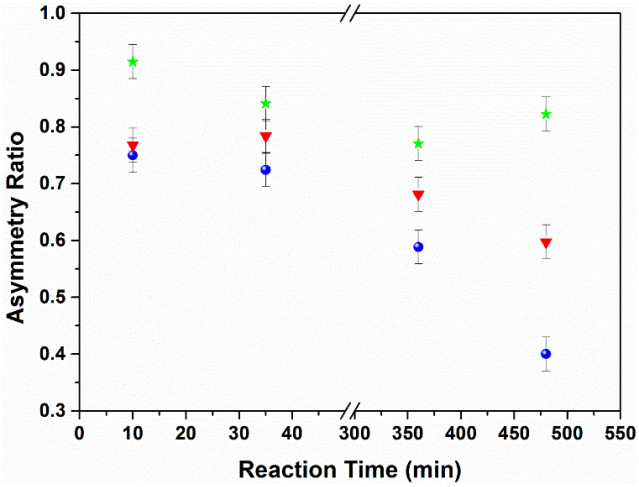

Figure 8. Asymmetry ratios for the CN samples (blue dots), CK samples (green stars), and SN samples (red triangles) synthesized at different reaction times (λ_{exc} = 461.0 nm).

For all samples under investigation, *R* tends to decrease when the reaction time increases. It is important to note that the behaviour of CaF_2 co-doped with Eu^{3+} and Na^+ is different from CaF_2 co-doped with Eu^{3+} and K^+ and from SrF_2 co-doped with Eu^{3+} and Na^+. In fact, *R* for the CN samples is always lower than *R* for the other samples. For the samples synthesized with 10 minute reaction time, CN10 and SN10 present almost the same *R* value, around 0.75, meaning that a similar average symmetry is present, while the *R* value for the CK10 sample is around 0.9. Also, the behaviour of *R* for the three kinds of sample are different when the reaction time increases.

For the CN samples there is a decrease of 47% between the value of *R* for the 10 min reaction time sample and the 8 hour reaction time sample, while for the CK samples, *R* presents a decrease of 10% and a 22% decrease for the SN samples.

Overall, it is possible to infer that by increasing the reaction time the symmetry of site 1 becomes higher. The main difference in the *R* behaviour is between the CN and the CK samples. Specifically, *R* for the CN samples undergoes a large decrease when the reaction time increases while for the CK samples, the decrease is much lower. This can be attributed to the different co-

doping ions, Na^+ for the CN samples and K^+ for the CK samples, that were used to compensate the extra charge of the Eu^{3+} when they substitute Ca^{2+} ions in the matrix.

In order to investigate the contribution of the different Stark sub-levels to the emission spectrum, emission measurements at 77 K were also carried out. The local symmetry of the Eu^{3+} ions can be investigated considering the number of transitions due to Stark splitting observed for the bands[16, 23, 29], since the number of the bands depends on the crystal field splitting due to the local lanthanide symmetry.

In Figure 9, the 77 K emission spectra for the CN480 sample under site selection are shown. The spectra for the other samples are shown in Figure S5 of the Supporting Information. The emission of the CN480 sample is shown since it is the only sample where site 1 can be perfectly selected by exciting at 461.0 nm. As can be observed in Figure 9, all the bands show a narrowing behavior with respect to the one at room temperature (Figure 7). As found also at room temperature, the $^5D_0 \rightarrow {}^7F_0$ transition for site 1 is not present, and therefore the one observed for excitation at 464.5 can be attributed only to site 2. This confirms that the Eu^{3+} ions accommodated in site 1 have a higher symmetry than the ones in site 2. Other well-defined narrow bands are visible for the $^5D_0 \rightarrow {}^7F_1$ and $^5D_0 \rightarrow {}^7F_2$ transitions in the 580 – 630 nm emission range. In Figure 11, a detailed section of the emission spectra is shown, presenting the emission bands of the $^5D_0 \rightarrow {}^7F_0$, $^5D_0 \rightarrow {}^7F_1$ and $^5D_0 \rightarrow {}^7F_2$ transitions. All the 77K emission spectra, shown in the Supporting Information, Figure S6, present the same spectral behavior as the CN480 sample, although some multiple site emission is present. For the low reaction time samples, the emission bands are broader.

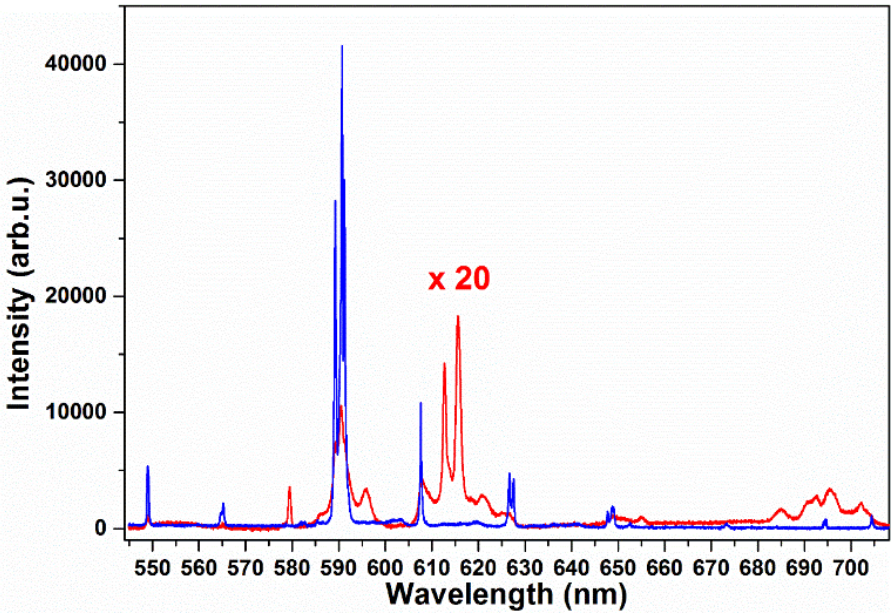

Figure 9. 77 K emission spectra for the CN480 sample. Blue line: λ_{exc} = 461.0 nm; Red line: λ_{exc} = 464.5 nm.

As it can be seen in Figure 10, the two sites present 3 bands for the $^5D_0 \rightarrow {}^7F_1$ transition around 590 nm. For site 2 the $^5D_0 \rightarrow {}^7F_0$ transition is present, therefore its possible site symmetry is restricted to C_{2v}, C_2, C_s or C_1[16, 29]. It is not possible to perfectly assign the symmetry of site 2 since it presents multiple site emission when excited at 464.5 nm, and the emission bands are not well resolved even at 77 K.

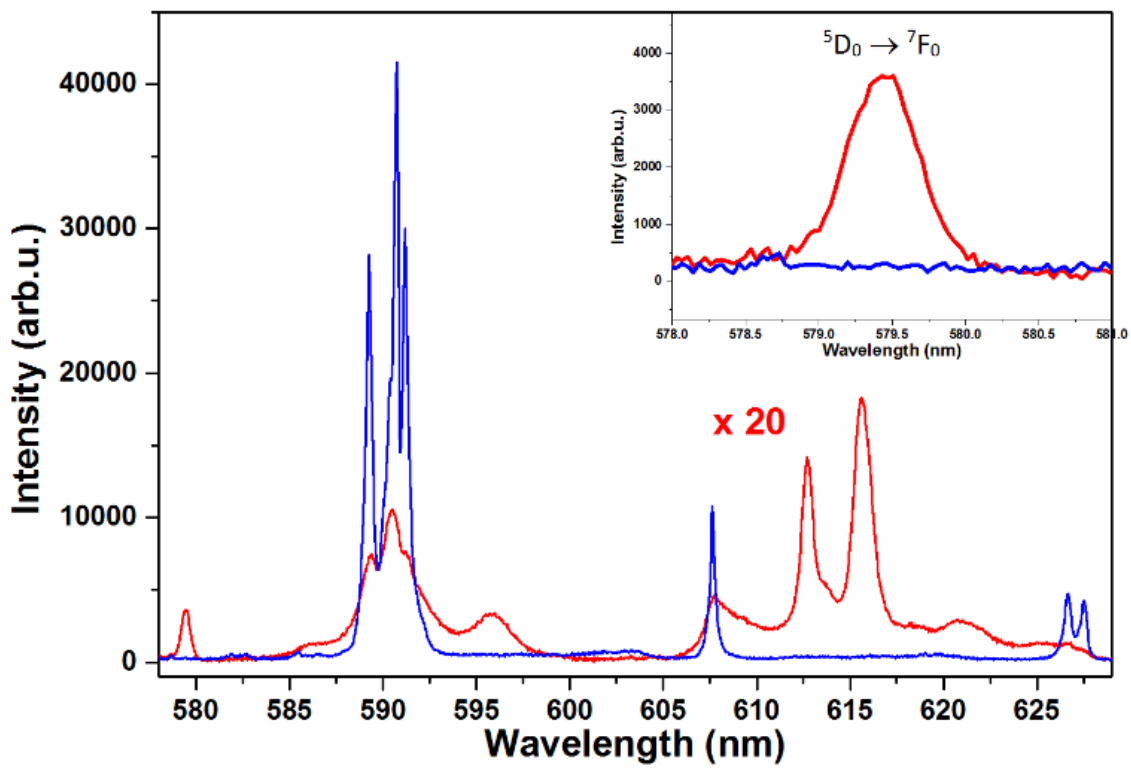

Figure 10. Emissions bands due to the $^5D_0 \rightarrow {}^7F_0$, $^5D_0 \rightarrow {}^7F_1$ and $^5D_0 \rightarrow {}^7F_2$ transitions for the CN480 sample at 77 K. Blue line: λ_{exc} = 461.0 nm; Red line: λ_{exc} = 464.5 nm. In the inset a zoom on the emission band of the $^5D_0 \rightarrow {}^7F_0$ transition, with site 1 emission magnified 20 times.

Like the room temperature emission spectra, site 1 presents no $^5D_0 \rightarrow {}^7F_0$ transition and three bands for the $^5D_0 \rightarrow {}^7F_2$ transition, the first at 607.5 nm, and the other 2 at 627 nm and 627.5 nm. The emission bands of the $^5D_0 \rightarrow {}^7F_2$ transition perfectly match those for the P site found by Hamers et al. in Eu^{3+} doped CaF_2 single crystals[15] with the same Stark splitting. It is worth noting that Hamers do not assign a symmetry for the P site. Since the $^5D_0 \rightarrow {}^7F_0$ transition is absent, and both the $^5D_0 \rightarrow {}^7F_1$ and $^5D_0 \rightarrow {}^7F_2$ transitions show three bands due to Stark splitting, it is possible to assign the $\mathbf{D_2}$ symmetry to site 1[16, 29]. As far as we know, this is the first time that a site with $\mathbf{D_2}$ symmetry has been found and assigned for Eu^{3+} ions in CaF_2 or SrF_2.

To confirm the results obtained, the lifetimes of the $^5D_0$ level for site 1 for all the samples were acquired and are shown in Figure 11. The $^5D_0$ state presents long lifetimes, as reported by Hamers et al. for the P site (16 ms)[15].

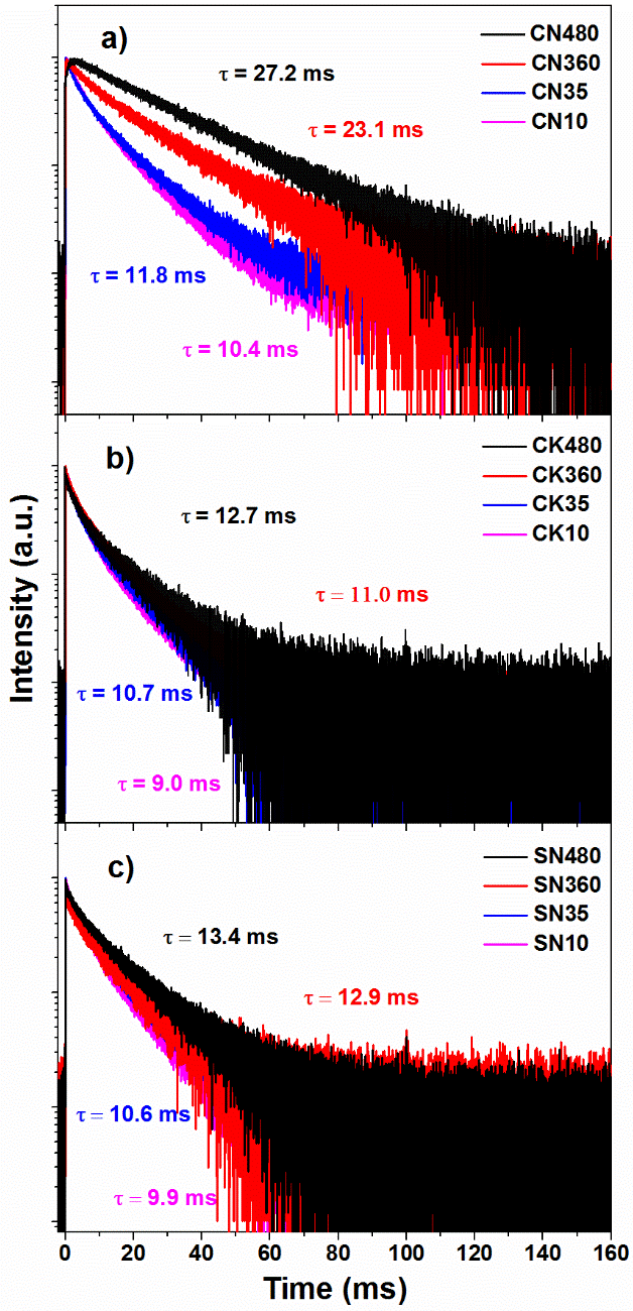

Figure 11 Decay times in logarithmic scale of the $^5D_0$ state, in the a) CN samples, in b) CK samples, in c) SN samples (λ_{exc}=461.0 nm)

Since the decay curves present a non-exponential behaviour (apart from the CN480 sample) the effective lifetime has been calculated using the formula[33]:

$$\tau_{eff} = \frac{\int_0^{Tmax} t \times I(t) dt}{\int_0^{Tmax} I(t) dt} \qquad (2)$$

where *I(t)* is the measured decay curve and $T_{max} >> \tau_{eff}$. For site 1, the $^5D_0$ state lifetime increases by increasing the reaction time, but for CK and SN (Figures 11b and 11c) only a slight difference in the lifetime of the different samples is present (it varies from 9.0 ms for CK10 to 12.7 ms for CK480 and from 9.9 ms for SN10 to 13.4 ms for SN480). For the CK and SN samples the decay curves do not present a single exponential behaviour, meaning that the emission is not from Eu^{3+} ions accommodated in a single site but probably from both site 1 and 2. Conversely, CN samples (Figure 11a) show a large difference between samples with different reaction times. Every CN sample at a defined reaction time presents a higher lifetime than the CK or SN sample with similar reaction time.

Furthermore, the difference between CN10, CN35, CN360 and CN480 is sharp. The lower lifetime for a CN sample is 10.4 ms (CN10), while it is 27.2 ms for the CN480 sample. To the best of our knowledge, a decay time of 27.2 ms is the longest decay time ever measured for the $^5D_0$ level of Eu^{3+}. Also the shape of the lifetime curve changes for CN depending on the reaction time: the behaviour of CN10 and CN35 resembles the behaviour of CK and SN samples, while CN360 and CN480 exhibit an almost single exponential behaviour. This confirms the behaviour of the emission obtained with site selection spectroscopy showing that for the CN480 sample, the emission from site 2 is almost disappeared. In fact, such a long lifetime means that Eu^{3+} is located in the site with higher symmetry (site 1, D_2 symmetry). The rise-decay behaviour that can be seen in the decay-time curves of the CN samples (especially for CN360 and CN480) can be ascribed to a slow $^5D_1 \rightarrow {}^5D_0$ feeding[33].

From the lifetime measurements, it is possible to infer that the contribution of site 1 to the overall emission increases when the synthesis reaction time increases. It is more evident for the CN samples, where the lifetime of the $^5D_0$ state shows an almost perfect exponential behaviour for the CN480 sample (confirmed also by the high emission intensity of site 1 with respect to site 2 as it can be seen in Figures 8, 10 and 11).

The comparison between the lifetimes of the CN and CK samples also confirms the ICP-MS results, since Na^+ ions can substitute Ca^{2+} ions at least two times more than K^+ ions, and the amount of Na^+ ions in the CN samples is similar to the amount of Eu^{3+} ions. Therefore, by increasing the reaction time, more Na^+ ions can be arranged in a D_2 symmetry around Eu^{3+} ions for the CN samples. This behaviour can be seen also for the CK and SN samples, but with less efficiency. Moreover, Na^+ is known to favour the presence of symmetric sites when co-doped with lanthanide ions[34].

3.4 Multiphoton spectroscopy

As a proof of concept, the possibility of using the NPs as optical probes in multiphoton spectroscopy was tested. In particular, the Eu^{3+} emission of the CN10 samples deposited on a microscope glass slide was measured after two-photon excitation with a two-photon microscope. The emission is shown in Figure 13, where the orange-red emission in the 570-650 nm range for the CN10 NPs can be easily observed upon 790 nm pulsed laser excitation.

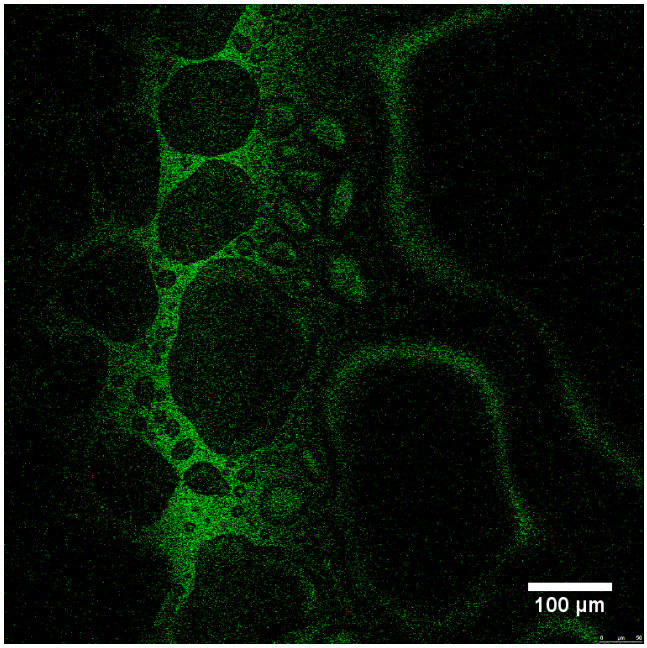

Figure 13. Two photon excitation image for the CN10 sample. λ_{exc} = 790 nm, λ_{emi} 570-650 nm.

The signal to noise ratio, obtained by setting the laser power at 29% of the maximum power, was found to be 3.9. In the images, the light signal appears homogeneous at 20x magnification in the regions covered by the NPs and still uniform up to an ulterior 5% of electronic zooming. Finally, the signal intensity was found compatible with biomedical applications focused on the imaging of histological specimens or for in vivo intravital microscopy.

CONCLUSIONS

Eu^{3+} doped CaF_2 and SrF_2 single phase NPs were prepared by a one-step, simple and environmental friendly hydrothermal technique. The NPs are easily dispersible in water solutions, without the need of any post-synthesis reaction. The size of the NPs can be tuned by changing the reaction time. Site selective laser spectroscopy was used to define the local symmetry properties of the Eu^{3+} ions in the different kinds of NPs and to investigate the relative populations of the

different sites by varying the reaction time. The $^5D_0$ level lifetime measured for the CN480 sample (27.2 ms) is the longest ever measured for Eu^{3+} ions. This leads to some possible applications in biomedicine, for time resolved imaging spectroscopy, to eliminate the autofluorescence of the biological tissues, for instance using Fluorescence Lifetime Imaging Microscopy.[35]

Preliminary multiphoton excitation measurements prove that these NPs could be useful for potential *in-vitro* as well *in-vivo* applications using NIR excitation in the first biological window.

Acknowledgements

University of Verona, in the framework of the "Ricerca di base" project is gratefully acknowledged for financial support. FV is grateful for financial support from the Natural Sciences and Engineering Research Council (NSERC) of Canada and the Fonds de recherche du Québec – Nature et technologies (FRQNT). PC is grateful for financial support from Ca' Foscari University of Venice ADIR-2016.

ASSOCIATED CONTENT

Supporting Information. The Supporting Information file is included.

AUTHOR INFORMATION

Corresponding Author

*Adolfo Speghini, Nanomaterials Research Group, Dipartimento di Biotecnologie, Università di Verona and INSTM, UdR Verona, Strada Le Grazie 15, I-37134 Verona, Italy, adolfo.speghini@univr.it

Author Contributions

The manuscript was written through contributions of all authors. All authors have given approval to the final version of the manuscript.

REFERENCES

(1) Hillhouse, H. W.; Beard, M. C., Solar cells from colloidal nanocrystals: Fundamentals, materials, devices, and economics. *Current Opinion in Colloid & Interface Science* **2009,** 14, (4), 245-259.

(2) Di, W.; Li, J.; Shirahata, N.; Sakka, Y.; Willinger, M. G.; Pinna, N., Photoluminescence, cytotoxicity and in vitro imaging of hexagonal terbium phosphate nanoparticles doped with europium. *Nanoscale* **2011,** 3, (3), 1263-9.

(3) Bunzli, J. C., Benefiting from the unique properties of lanthanide ions. *Accounts of chemical research* **2006,** 39, (1), 53-61.

(4) Ma, Z. Y.; Dosev, D.; Nichkova, M.; Gee, S. J.; Hammock, B. D.; Kennedy, I. M., Synthesis and bio-functionalization of multifunctional magnetic Fe_3O_4@Y_2O_3:Eu nanocomposites. *Journal of materials chemistry* **2009,** 19, (27), 4695-4700.

(5) Dong, N. N.; Pedroni, M.; Piccinelli, F.; Conti, G.; Sbarbati, A.; Ramirez-Hernandez, J. E.; Maestro, L. M.; Iglesias-de la Cruz, M. C.; Sanz-Rodriguez, F.; Juarranz, A.; Chen, F.; Vetrone, F.; Capobianco, J. A.; Sole, J. G.; Bettinelli, M.; Jaque, D.; Speghini, A., NIR-to-NIR two-photon excited CaF_2:Tm^{3+},Yb^{3+} nanoparticles: multifunctional nanoprobes for highly penetrating fluorescence bio-imaging. *ACS nano* **2011,** 5, (11), 8665-71.

(6) Reisfeld, R., New developments in luminescence for solar energy utilization. *Optical Materials* **2010,** 32, (9), 850-856.

(7) Dong, H.; Sun, L. D.; Yan, C. H., Energy transfer in lanthanide upconversion studies for extended optical applications. *Chem. Soc. Rev.* **2015,** 44, (6), 1608-1634.

(8) Naccache, R.; Yu, Q.; Capobianco, J. A., The Fluoride Host: Nucleation, Growth, and Upconversion of Lanthanide-Doped Nanoparticles. *Adv. Opt. Mater.* **2015,** 3, (4), 482-509.

(9) van der Ende, B. M.; Aarts, L.; Meijerink, A., Lanthanide ions as spectral converters for solar cells. *Physical chemistry chemical physics : PCCP* **2009,** 11, (47), 11081-95.

(10) Chatterjee, D. K.; Rufaihah, A. J.; Zhang, Y., Upconversion fluorescence imaging of cells and small animals using lanthanide doped nanocrystals. *Biomaterials* **2008,** 29, (7), 937-43.

(11) Kemnitz, E.; Ritter, B.; Krahl, T.; Rurack, K., Nanoscale CaF_2 doped with Eu^{3+} and Tb^{3+} through fluorolytic sol-gel-synthesis. *J. Mater. Chem. C* **2014**.

(12) Dolcet, P.; Mambrini, A.; Pedroni, M.; Speghini, A.; Gialanella, S.; Casarin, M.; Gross, S., Room temperature crystallization of highly luminescent lanthanide-doped CaF_2 in nanosized droplets: first example of the synthesis of metal halogenide in miniemulsion with effective doping and size control. *RSC Adv*. **2015,** 5, (21), 16302-16310.

(13) Cirillo-Penn, K. M.; Wright, J. C., Laser spectroscopic measurement of point-defect dynamics in Eu^{3+}:CaF_2. *Physical Review B* **1990,** 41, (15), 10799-10807.

(14) Laval, J. P.; Mikou, A.; Frit, B.; Roult, G., Short-range order in heavily doped CaF_2:Ln^{3+} fluorites: A powder neutron diffraction study. *Solid State Ionics* **1988,** 28-30, 1300-1304.

(15) Hamers, R. J.; Wietfeldt, J. R.; Wright, J. C., Defect Chemistry in CaF_2-Eu^{3+}. *J Chem Phys* **1982,** 77, (2), 683-692.

(16) Ju, Q.; Liu, Y.; Li, R.; Liu, L.; Luo, W.; Chen, X., Optical Spectroscopy of Eu^{3+}-Doped BaFCl Nanocrystals. *The Journal of Physical Chemistry C* **2009,** 113, (6), 2309-2315.

(17) Jouart, J. P.; Bissieux, C.; Mary, G.; Egee, M., A spectroscopic study of Eu^{3+}centres in SrF_2using a site-selective excitation technique. *Journal of Physics C: Solid State Physics* **1985,** 18, (7), 1539-1551.

(18) Werts, M. H. V.; Jukes, R. T. F.; Verhoeven, J. W., The emission spectrum and the radiative lifetime of Eu^{3+} in luminescent lanthanide complexes. *Physical Chemistry Chemical Physics* **2002,** 4, (9), 1542-1548.

(19) Ritter, B.; Haida, P.; Fink, F.; Krahl, T.; Gawlitza, K.; Rurack, K.; Kemnitz, E., Novel and Easy Access to Highly Luminescent Eu and Tb Doped Ultra-small CaF_2, SrF_2 and BaF_2 Nanoparticles – Structure and Luminescence. *Dalton Trans*. **2017**.

(20) Pedroni, M.; Piccinelli, F.; Passuello, T.; Polizzi, S.; Ueda, J.; Haro-González, P.; Martinez Maestro, L.; Jaque, D.; García-Solé, J.; Bettinelli, M.; Speghini, A., Water (H_2O and D_2O) Dispersible NIR-to-NIR Upconverting Yb^{3+}/Tm^{3+}Doped MF_2(M = Ca, Sr) Colloids: Influence of the Host Crystal. *Crystal Growth & Design* **2013,** 13, (11), 4906-4913.

(21) Wells, J.-P. R.; Reeves, R. J., Polarized laser selective excitation and Zeeman infrared absorption of C_{4v} and C_{3v} symmetry centers in Eu^{3+}- doped CaF_2, SrF_2, and BaF_2 crystals. *Physical Review B* **2001,** 64, (3).

(22) Wells, J.-P. R.; Reeves, R. J., Polarized laser-selective excitation and Zeeman infrared absorption of Sm^{3+} centers in CaF_2 and SrF_2 crystals. *Physical Review B* **2000,** 61, (20), 13593-13608.

(23) Gastev, S. V.; Choi, J. K.; Reeves, R. J., Laser spectroscopy of Eu^{3+} cubic centers in the CaF_2 bulk single crystal. *Physics of the Solid State* **2009,** 51, (1), 44-49.

(24) Jones, G. D.; Reeves, R. J., Na^+, Li^+ and cubic centres in rare-earth-doped CaF_2 and SrF_2. *Journal of Luminescence* **2000,** 87-89, 1108-1111.

(25) Martin, P.; Hamaidia, A.; Margerie, J., Paramagnetic colour centres in SrF_2:Na^+. *Journal of Physics C: Solid State Physics* **1985,** 18, (32), 5947-5961.

(26) Su, L.; Xu, J.; Li, H.; Yang, W.; Zhao, Z.; Si, J.; Dong, Y.; Zhou, G., Codoping Na^+ to modulate the spectroscopy and photoluminescence properties of Yb^{3+} in CaF_2 laser crystal. *Opt. Lett.* **2005,** 30, (9), 1003.

(27) Shannon, R. D., Revised effective ionic radii and systematic studies of interatomic distances in halides and chalcogenides. *Acta Crystallographica Section A* **1976,** 32, (5), 751-767.

(28) Su, L.; Xu, J.; Li, H.; Wen, L.; Zhu, Y.; Zhao, Z.; Dong, Y.; Zhou, G.; Si, J., Sites structure and spectroscopic properties of Yb-doped and Yb, Na-codoped CaF_2 laser crystals. *Chemical Physics Letters* **2005,** 406, (1-3), 254-258.

(29) Binnemans, K., Interpretation of europium(III) spectra. *Coordination Chemistry Reviews* **2015,** 295, 1-45.

(30) Sarkar, S.; Hazra, C.; Mahalingam, V., Bright luminescence from colloidal Ln^{3+}-doped $Ca_{0.72}Y_{0.28}F_{2.28}$ (Ln=Eu, Tm/Yb) nanocrystals via both high and low energy radiations. *Chemistry* **2012,** 18, (23), 7050-4.

(31) Das, S.; Amarnath Reddy, A.; Ahmad, S.; Nagarajan, R.; Vijaya Prakash, G., Synthesis and optical characterization of strong red light emitting $KLaF_4$:Eu^{3+} nanophosphors. *Chemical Physics Letters* **2011,** 508, (1-3), 117-120.

(32) Song, L.; Gao, J.; Song, R., Synthesis and luminescent properties of oleic acid (OA)-modified CaF_2: Eu nanocrystals. *Journal of Luminescence* **2010,** 130, (7), 1179-1182.

(33) Passuello, T.; Piccinelli, F.; Trevisani, M.; Giarola, M.; Mariotto, G.; Marciniak, L.; Hreniak, D.; Guzik, M.; Fasoli, M.; Vedda, A.; Jary, V.; Nikl, M.; Causin, V.; Bettinelli, M.; Speghini, A., Structural and optical properties of Vernier phase lutetium oxyfluorides doped with lanthanide ions: interesting candidates as scintillators and X-ray phosphors. *Journal of materials chemistry* **2012,** 22, (21), 10639.

(34) Hraiech, S.; Jouini, A.; Jin Kim, K.; Guyot, Y.; Yoshikawa, A.; Boulon, G., Role of monovalent alkali ions in the Yb^{3+} centers of CaF_2 laser crystals. *Radiation Measurements* **2010,** 45, (3-6), 323-327.

(35) Siegel, J.; Elson, D. S.; Webb, S. E. D.; Lee, K. C. B.; Vlandas, A.; Gambaruto, G. L.; Lévêque-Fort, S.; Lever, M. J.; Tadrous, P. J.; Stamp, G. W. H.; Wallace, A. L.; Sandison, A.; Watson, T. F.; Alvarez, F.; French, P. M. W., Studying Biological Tissue with Fluorescence Lifetime Imaging: Microscopy, Endoscopy, and Complex Decay Profiles. *Applied Optics* **2003,** 42, (16), 2995.